Acta Oceanol. Sin., 2020, Vol. 39, No. 10, P. 96–106
https://doi.org/10.1007/s13131-020-1679-9
http://www.hyxb.org.cn
E-mail: hyxbe@263.net

The controlling factors of high suspended sediment concentration in the intertidal flat off the Huanghe River Estuary

Bowen Li[1, 3], Yonggang Jia[1, 2*], J. Paul Liu[3], Jianfeng Su[3, 4], Xiaolei Liu[1, 2], Mingzheng Wen[5]

[1] Shandong Provincial Key Laboratory of Marine Environment and Geological Engineering, Ocean University of China, Qingdao 266100, China

[2] Laboratory for Marine Geology, Pilot National Laboratory for Marine Science and Technology (Qingdao), Qingdao 266237, China

[3] Department of Marine, Earth and Atmospheric Sciences, North Carolina State University, Raleigh, NC 27695, USA

[4] State Key Laboratory of Marine Geology, Tongji University, Shanghai 200092, China

[5] Tianjin Center, China Geological Survey, Tianjin 300170, China

Received 21 May 2020; accepted 29 June 2020

Abstract

The Huanghe River (Yellow River) is known by its high suspended sediment concentration (SSC) in its river mouth tidal flat. However, the factors controlling the high SSC over there are not well understood. Therefore, we conducted 7-d hydrodynamic observations (water depth, wave height, and current velocity) and SSC measurements on the tidal flat off the Huanghe River Mouth. The data shows that in most of time, under the calm sea condition, the SSC ranges 0.1–3.5 g/L, and sediment discharge from the river is the main source. However, when hydrodynamics are enhanced in a tidal cycle and large-scale erosion occurs on the seafloor, resuspended sediment becomes the main source, and the SSC in the water column reaches 17.3 g/L. We find the suspended sediment flux is mainly controlled by the tidal current and Stokes drift, while the wave-induced shear stress could also affect the variation of suspended sediment flux. During the observation period, when sea under calm-rippled conditions, the current-induced resuspended sediment concentration (RSC) was greater than the wave-induced RSC. In contrast, in smooth-wavelet sea conditions, the wave-induced RSC was greater than the current-induced RSC, for instance, a single wave event was found to cause 11.8 cm seabed erosion within 6 h. This study reveals different controlling factors for the high SSC near a river-influenced tidal flat, and helps us get a better understanding of a delta's depositional and erosional mechanisms.

Key words: Huanghe River (Yellow River), sediment re-suspension, sediment transport, wave, current, *in-situ* observation

Citation: Li Bowen, Jia Yonggang, Liu J. Paul, Su Jianfeng, Liu Xiaolei, Wen Mingzheng. 2020. The controlling factors of high suspended sediment concentration in the intertidal flat off the Huanghe River Estuary. Acta Oceanologica Sinica, 39(10): 96–106, doi: 10.1007/s13131-020-1679-9

1 Introduction

Suspended sediments are an important part of sediment movement in estuarine-coastal waters. Their distribution, diffusion, and deposition have a major impact on ports, waterways, and ecological environments. Therefore, temporal changes in the suspended sediment concentration (SSC) are an important issue in estuarine-coastal research. Previous studies have suggested that SSC variations in estuarine waters are significantly affected by flood and ebb tides, spring and neap tides, and seasonal factors (Chen et al., 2004; Kong et al., 2006; Wan et al., 2006; Zuo et al., 2006). High SSC is normally the result of the combined effects of sediment transport and resuspension (Ramaswamy et al., 2004).

Tidal current and Stokes drift usually dominate the suspended sediment transport (Chen et al., 2009). There is a high correlation between the coastal SSC and mean tidal current velocity in tidal channels (Chen et al., 2017; Wu et al., 2006). SSC changes in the vertical profile are normally related to sediment transported by tidal, which carries a large number of suspended sediments, resulting in an increase of SSC in the 0.5 m-thick layer of water above the sea bed (Li et al., 1998a, b). Furthermore, sediment resuspension is another source of suspended particulate matter in the water near the seabed (Zhou et al., 2009; Zhang et al., 2004, 2005).

Some studies have found that storms have a significant effect on sediment resuspension on the shelf and near the river mouth (Chen et al., 2003a, b; Kineke and Sternberg, 1992; Rose and Thorne, 2001; Shi and Ling, 1999; Shi et al., 1985; Sternberg et al., 1999). Currents and waves are found as the main hydrodynamic factors inducing seabed sediment resuspension in estuarine water (Lavelle et al., 1984; Roman and Tenore, 1978). At shallow shelf (<20 m) environments, waves can easily resuspend the

Foundation item: The National Natural Science Foundation of China under contract Nos 41072215 and 41877223; the Key Science and Technology Plan of Power China Huadong Engineering Corporation Limited under contract No. KY2018-ZD-01; the Joint Fund of NSFC and Marine Science Research Centers of Shandong Province of China under contract No. U1906230; the Marine Geological Survey Project of the China Geological Survey under contract No. GZH201100203.
*Corresponding author, E-mail: yonggang@ouc.edu.cn

seabed sediment and significantly enhance the SSC (Thompson et al., 2011; Wright et al., 1992, 1997; You, 2005). Therefore, waves may become the main factor controlling sediment resuspension (Green, 2011; You, 2005). However, when wave height is low, tidal currents play major roles on resuspension (Janssen-Stelder, 2000).

The Huanghe River (Yellow River) Estuary is a typical hyperconcentrated estuary in the world. Previous studies find that the sediment in the Huanghe River Estuary was resuspended by storm and strong tidal currents, resulting in high density gravity flow (Wright et al., 1988) and underwater slope failure (Prior et al., 1989). Tidal current has a major impact on the suspended sediment distribution and transport in the Huanghe River Estuary (Li et al., 1998a). Sediment concentration changes in the vertical are related to sediment flux from the river (Li et al., 1998b). However, it is still not clear how much of the high SSC is induced by local resuspension and how much is directly induced by sediment flux from the river.

In summary, reususpension induced by waves or tides and sediment transported by rivers are main source of suspended sediment. In order to accurately analyze the effect of local shear stress on bed sediments, the SSC needs to be decomposed into resuspended sediment concentration and transport sediment concentration. The suspended sediment transport flux is the most important indicator of suspended sediment diffusion and transportation. To accurately estimate the sediment flux, it must be based on the observation of the SSC profile of the water column, because the SSC in the water column varies greatly even under the strong mixing condition. For example, in the Wadden Sea in Denmark, Pejrup (1988) found that when the SSC is low (average concentration is about 80 mg/L), the SSC is evenly distributed between 50 cm and 100 cm above the bottom bed; when the SSC is high (average concentration is about 160 mg/L), the SSC decreases with the increase of the bed distance. Nonetheless, most researchers assume that the SSC is uniform in the water profile to calculating the suspended sediments flux. For example, Andersen and Pejrup (2001) calculated the suspended sediment flux in the Wadden Sea in Denmark. Compared with the open coastal intertidal zone, the problem of the river estuary is more difficult to solve, because the estuary usually has a lower deposition rate, so suspended sediments can be suspended in the water column for a long time and transported by current to other locations.

Based on 7-d observation data, this paper try to decompose the SSC to analyzing the relationship between SSC change with hydrodynamic and suspended sediment flux during tidal cycles. The sediment transport and resuspension mechanisms in Huanghe River Delta are further revealed.

2 Study site

Historically the Huanghe River contributes 1×10^9 t/a fluvial sediment to the ocean (Ren and Shi, 1986; Wang and Aubrey, 1987), and its delta has a high rate of deposition. The average SSC near the river mouth is approximately 2.5 g/L (Wright and Nittrouer, 1995). The sea normally is much rougher during the winter monsoon season than the summer season, correspondingly the SSC in the winter are significantly higher than that in summer season, sometimes the SSC in winter are 20 times than in summer (Yang et al., 2011). The median particle size of the sediment on the seabed is 0.036 mm, and the density is 1.96–1.97 g/cm^3. The surface sediment void ratio is 0.73–0.76, and the water content is 26.2%–27.9% (Liu et al., 2013).

The area selected for *in-situ* measurement (38°01′N, 118°57′E) is located in the intertidal flat off the Huanghe River Estuary (Fig. 1). Previous studies indicate the occurrence of resuspension in the research area is very high (Zhao, 2004; Zong, 2009). The tidal characteristic is irregular semidiurnal tide, the average tidal range is 0.7–1.7 m, and the maximum tidal range is

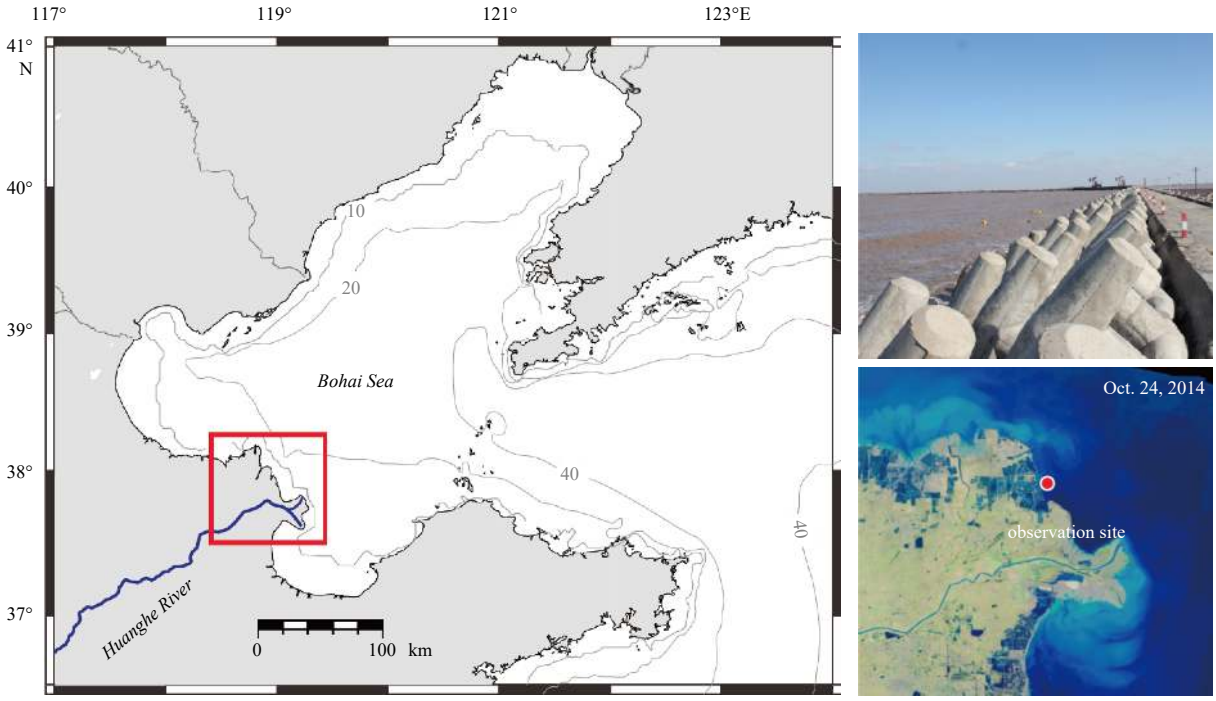

Fig. 1. Study area and location of the *in-situ* observation site off the Huanghe River Estuary, China. The photograph shows the intertidal zone is submerged at high tide, and the Landsat Satellite image in October 24, 2014 shows the high SSC off the Huanghe River Mouth.

2.17 m. Tidal current is the main current; the maximum velocity is more than 140 cm/s. The wave height is generally less than 0.5 m, while wave height may be up to 3–5 m under extreme sea conditions (Cheng and Xue, 1997).

3 Methods

3.1 *Observation instrument*

To measure erosion and deposition, current velocities, and turbidity we mounted a pack of sediment and hydrodynamic instruments on a tripod deployed at the middle of the intertidal zone, including autonomous altimeter, current-velocity meter, Argus surface meter, turbidity meter and wave tide gauge (see details in Fig. 2). The distance from autonomous altimeter (AA400) to the seabed is 20 cm, its range is 0–3 000 mm, and the instrumental error is 2%. The sampling frequency is 1.0 Hz, and the sampling interval is 30 min. The distance from ALEC-EM current-velocity meter to the seabed is 10 cm, its range, accuracy, and direction are 0–500 cm/s, 1.0 cm/s, and the east, respectively, while the sampling frequency and interval are 1.0 Hz and 10 min, respectively. The Argus surface meter (ASM-4) touches the seabed including tilt sensors, temperature sensors, microcontrollers, a memory stick, a power supply, and a sensor stick with a length of 96 cm and sensor spacing of 1 cm; the range is 0–2 000 NTU, and the sampling interval is 15 min. The distance from XR-420 turbidity meter to the seabed is 10 cm, its range and instrumental error are 0–4 000 NTU and 2%, respectively, while the sampling frequency and interval are 1 Hz and 2 min, respectively. The distance from wave tide gauge (RB16-TWR-2 050) to the seabed is 20 cm, and its range and instrumental error are 0–25 m and 0.05%, respectively. This gauge measures the water pressure every 30 min with a sampling frequency of 1 Hz.

The distance from Argus surface meter (ASM-4), ALEC-EM current-velocity meter, XR-420 turbidity meter, autonomous altimeter (AA400) and wave tide gauge (RB16-TWR-2 050) to the seabed is 0 cm, 10 cm, 10 cm, 20 cm and 20 cm, respectively. The observation period was from September 17 to 24, 2014, of which between 21:00 September 21 to 21:00 September 22 no data was recorded due to storage card switch. The autonomous altimeter only recorded the seabed variation data between September 17 and 22. Except the 24 h no data window and water depth less than 20 cm, we collected SSC, wave height, current velocity and water level for the whole observation period.

3.2 *Data calculation and analysis*

The wave-induced shear stress was calculated by

$$\tau_{\mathrm{wmax}} = 0.5\rho_{\mathrm{w}} f_{\mathrm{w}} U_{\mathrm{max}}^2 \tag{1}$$

(Lund-Hansen et al., 1997), where τ_{wmax} is the maximum wave-induced shear stress (Pa); ρ_{w} is seawater density, assumed to be 1.025 g/cm^3; f_{w} is the wave friction coefficient, assumed to be 0.01 (Wright et al., 1990); and U_{max} is the maximum wave orbital velocity (m/s). The current-induced shear stress was calculated as

$$\tau_{\mathrm{c}} = C_{\mathrm{d}}\rho_{\mathrm{w}} U_{\mathrm{c}}^2 \tag{2}$$

(Lund-Hansen et al., 1997), where τ_{c} is the current-induced shear stress (Pa); C_{d} is the traction coefficient, which is assumed to be 3.1×10^{-3} (Wright et al., 1990); and U_{c} is the observed current velocity (m/s).

In the research region, the direction of waves is similar to that of currents as they are induced by wind. The current induced by current occupies the dominant position in the Huanghe River Delta (Wang et al., 2011). The direction of flood-tide current is southeast, and the direction of ebb-tide current is generally northwest (Hu et al., 1996), which is consistent with the strong summer wind direction (Ren et al., 2017). Therefore, the total shear stress could be express as the sum of the wave- and current-induced shear stresses (Li et al., 2020a):

$$\tau = \tau_{\mathrm{wmax}} + \tau_{\mathrm{c}} \tag{3}$$

(Grant and Madsen, 1979), where τ is the total stress (Pa), τ_{wmax} is the maximum of wave-induced shear stress (Pa), and τ_{c} is cur-

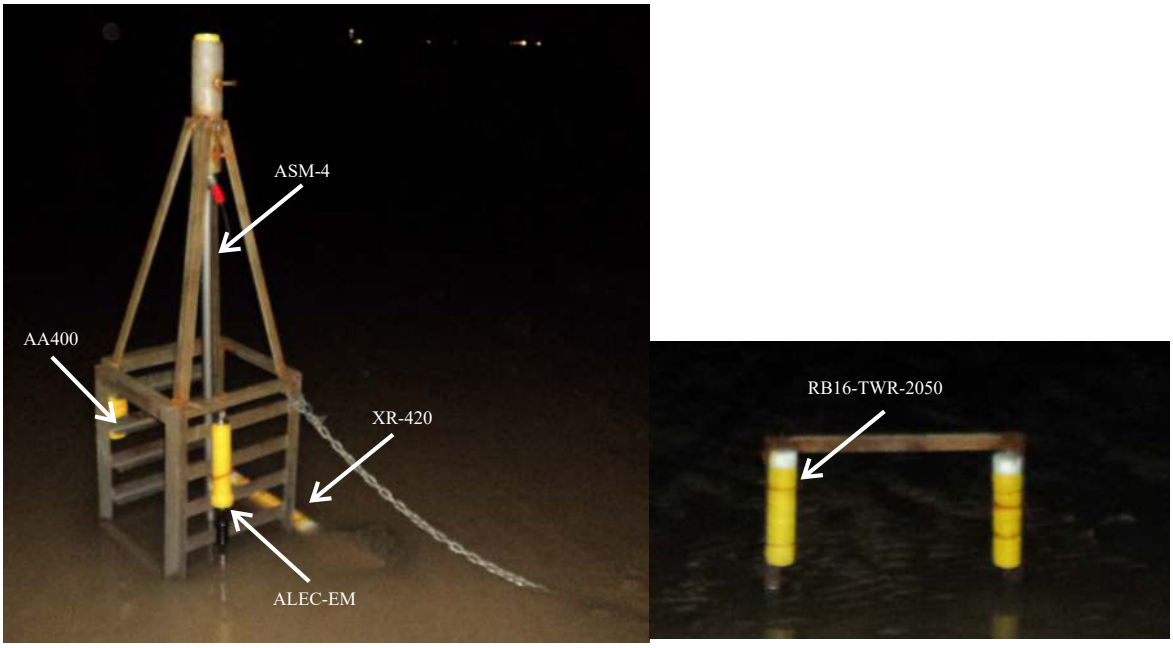

Fig. 2. Observation instruments and deployed observation system.

rent-induced shear stress (Pa).

We decompose unit width sediment loads (He and Sun, 1996; Wu et al., 2006) to distinguish SSCs induced by resuspension or sediment transport. The per-tidal-cycle current velocity, water depth, and suspended sediment content are decomposed into mean and pulsating values. The single-wide load can be expressed as

$$\begin{aligned} T =& VCH = (\bar{V}+V')(\bar{C}+C')(\bar{H}+H') \\ =& \bar{V}\bar{C}\bar{H} + V'C'\bar{H} + V'\bar{C}H' + V'\bar{C}\bar{H} + \bar{V}\bar{C}H' \\ &+ \bar{V}C'\bar{H} + \bar{V}C'H' + V'C'H' \end{aligned} \tag{4}$$

(Jay et al., 1997), where T is the single-wide sediment load (mg/(cm·s)), C is the SSC (g/L), V is the current velocity (cm/s), and H is the water depth (cm). $\bar{V}$, $\bar{C}$, and $\bar{H}$ are the average values of the depth-averaged current velocity, water depth, and depth-averaged SSC, respectively; and V', C', and H' are the pulsating values of the current velocity, water depth, and SSC, respectively. Over a single tide cycle, $\sum A' = \sum C' = \sum H'$. The single-wide load during a tide cycle can be expressed as

$$\begin{aligned} T &= \bar{V}\bar{C}\bar{H} + V'C'\bar{H} + V'\bar{C}H' + \bar{V}C'H' + V'C'H' \\ &= T_1 + T_2 + T_3 + T_4 + T_5, \end{aligned} \tag{5}$$

where C and H are positive constants, and V may be positive or negative. When V is positive, it is the flood-tidal current velocity, and when V is negative, it is the ebb-current velocity. T_1 and T_3 are the contributions of the advection transport volume and Stokes drift, and the sum of T_1 and T_3 is the transport volume. T_2, T_4, and T_5 are components of C', and the sediment concentration in water can be approximated as a constant during a tide cycle. The values of C' are affected by the two-way exchange of sediment between the sediment and water. The sum of T_2, T_4, and T_5 is the resuspended sediment volume.

The suspended sediment content can be expressed:

$$\sum_{i=1}^{H} C_i = CH, \tag{6}$$

where C_i is the SSC at different depths (g/L). From Eqs (7) and (9), the RSC can be expressed as

$$T_2 + T_4 + T_5 = C_\mathrm{r}VH, \tag{7}$$

$$C_\mathrm{r}VH/CVH = (T_2 + T_4 + T_5)/T, \tag{8}$$

$$C_\mathrm{r} = (T_2 + T_4 + T_5)\sum_{i=1}^{H} C_i/T, \tag{9}$$

where C_r is the RSC (g/L). From the above formulas, the transport sediment concentration can be calculated as

$$C_\mathrm{a} = T_1 \sum_{i=1}^{H} C_i/T, \tag{10}$$

$$C_\mathrm{s} = T_3 \sum_{i=1}^{H} C_i/T, \tag{11}$$

$$C_\mathrm{t} = C_\mathrm{a} + C_\mathrm{s}, \tag{12}$$

where C_a is the advection transport sediment concentration (g/L), C_s is the Stokes drift transport sediment concentration (g/L), and C_t is the transport sediment concentration (g/L). Using the above formulas, the suspended sediment content and contribution of current transport (tidal current and Stokes drift) and resuspension to the suspended sediment content can be calculated.

The critical shear stress was calculated by the equation (Wang et al., 2007) as fallow:

$$U_\mathrm{c} = \left(\frac{h}{d}\right)^{\frac{1}{7}} \left(17.6\frac{\gamma_\mathrm{s}-\gamma}{\gamma}d + 0.000\,000\,275\gamma_\mathrm{s}^{0.8}\frac{10+h}{d^{0.331}\gamma_\mathrm{s}^{0.8}}\right)^{\frac{1}{2}}, \tag{13}$$

where h is depth (m), γ_s is sediment density (g/cm^3), γ is water density (g/cm^3), d is medium diameter (mm) of sediment. When the erosion occurred, the depth is about 0.97 m, the sediment density is 1.97 g/cm^3, the water density is 1.03 g/cm^3, and the medium diameter of sediment is 0.036 mm. The calculated critical shear stress is 0.21 Pa.

The correlation between SSC and turbidity from the same ASM-4 and seabed sediment (Guo et al., 2016) can be expressed as

$$C = 0.008\,93t, \tag{14}$$

where t is turbidity (NTU).

4 Results

4.1 *Hydrodynamics parameters*

During the observation, at the observation site, sea conditions were mainly calm-rippled to smooth-wavelet (Fig. 3). The conditions are calm-rippled during the period from 10:00 on September 18 to 22:00 on September 20 and the period from 8:00 to 20:00 on September 23, while the other time are smooth-wavelet condition. The *in-situ* observations of hydrodynamic parameters during the period from September 17 to 24, 2014 are shown in Figs 3 and 4. The tidal range was 0.12–1.3 m and the water depth was between 0.16–1.51 m. Under the calm-rippled condition, the lowest water level was 0.16 m; the maximum water depth was less than 1.0 m and the effective wave height was generally 0–0.05 m. The maximum of current velocity was less than 20 cm/s. The hydrodynamic action enhanced under smooth-wavelet condition. During this time, the maximum of current velocity was 38.6 cm/s and the maximum of effective wave height was 0.51 m. The average current velocities during each tide cycle are shown in Table 1.

4.2 *Seabed variation*

During the observation period, the different impact of erosion and deposition on the seabed resulted in a relative change in the seabed observed by AA400 (Fig. 5). During the calm-rippled sea condition days, the seabed was deposited before 3:00 September 19, and transferred into slight erosion until 22:00 September 20, with a positive 38 mm seabed variation. When the first smooth-wavelet condition began to prevail at 22:00 September 20, the seabed suffered dramatically erosion with an erosion rate of 20.0 mm/h. The maximum of seabed variation during the observation period was 170 mm, and the total net erosion depth dur-

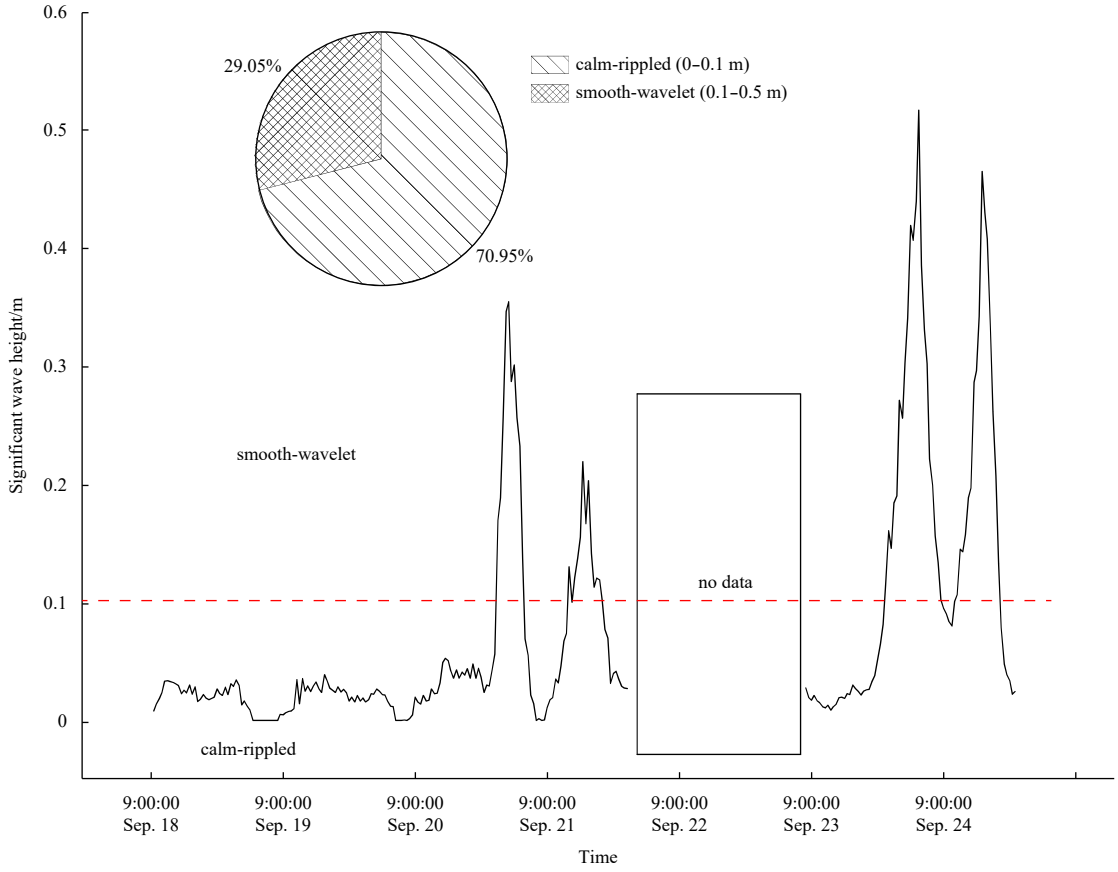

Fig. 3. Time percentage of different sea conditions during period from September 18 to 24, 2014.

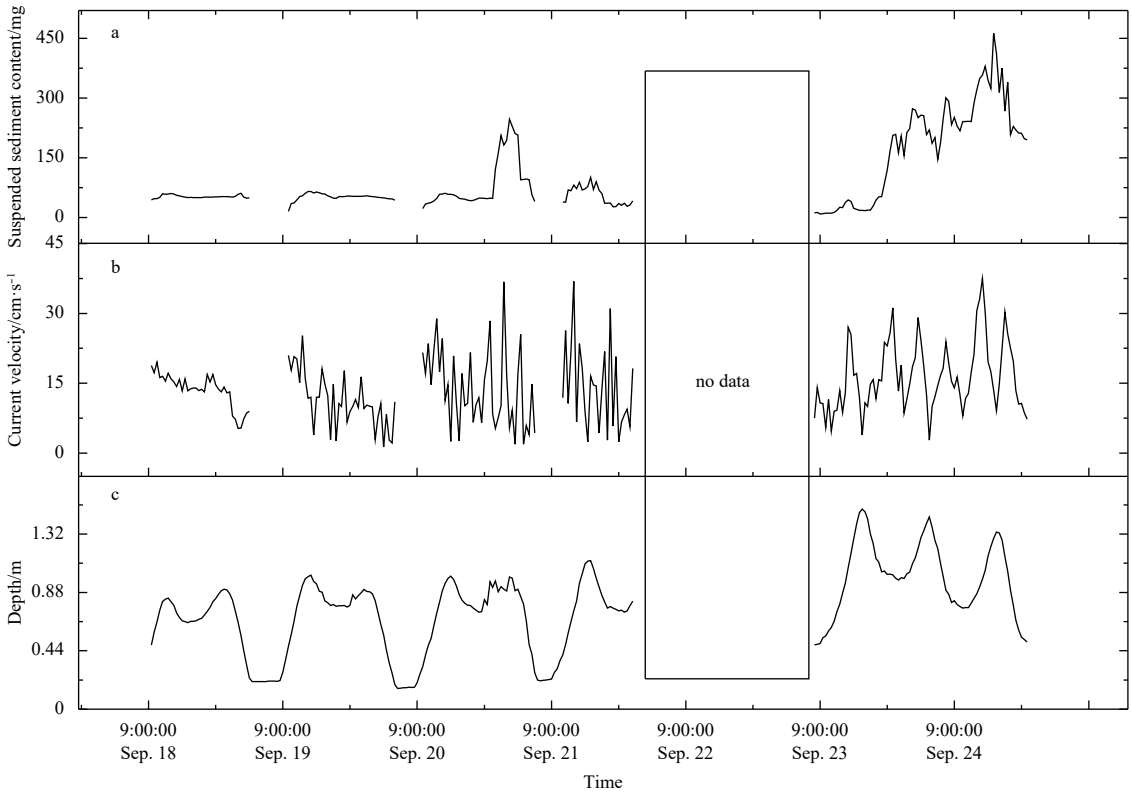

Fig. 4. Sediment content changes with hydrodynamic characteristic sediment content (a), current velocity (b), and depth of water (c) during the period of *in-situ* observation from September 18 to 24.

Table 1. The unit width sediment transport flux, transport volume and re-suspension during the observation period

Time	Average velocity /cm·s^{-1}	Unit width sediment transport flux /mg·cm^{-1}·s^{-1}	Advection transport volume /mg·cm^{-1}·s^{-1}	Stokes drift volume /mg·cm^{-1}·s^{-1}	Transport volume /mg·cm^{-1}·s^{-1}	Re-suspension /mg·cm^{-1}·s^{-1}
9:30–17:00 Sep. 18	–0.69	–51.36	–36.71	–2.04	–38.75	–12.61
17:30 Sep. 18 to 3:00 Sep. 19	2.69	131.65	156.56	43.33	199.89	–68.25
10:00–18:00 Sep. 19	2.32	16.19	119.64	–54.71	64.93	–48.74
18:30 Sep. 19 to 5:00 Sep. 20	1.63	98.34	96.90	86.74	183.64	–85.30
10:00–19:30 Sep. 20	1.97	69.74	96.92	–63.26	33.66	36.09
20:00 Sep. 20 to 6:00 Sep. 21	2.35	–31.69	277.28	124.43	401.71	–433.40
11:00–19:00 Sep. 21	3.00	173.45	202.73	–125.15	77.58	95.87
8:00–23:30 Sep. 23	2.66	–455.17	143.98	–82.25	61.73	–516.90
0:00–10:30 Sep. 24	0.15	96.87	476.20	36.67	512.87	–416.00
11:00–22:00 Sep. 24	0.86	666.07	256.67	157.42	414.09	251.98

ing the 4 d was 118 mm (Fig. 5).

4.3 *Sediment concentration*

The suspended sediment in the water column is found to correlate to seabed variation (Fig. 5). During the calm-rippled, the SSC observed by ASM-4 in the bottom water (the distances from the ground less than 30 cm) changed lightly, and the maximum of SSC was less than 5 g/L (Figs 6a–c). After 22:30 on September 20, the bottom water SSC increased obviously, and reached the maximum at 12.82 g/L after 3-h increasing. At 4:30 on September 21, it decreased to less than 4.8 g/L. During the 22:00 on September 23 to 22:00 on September 24, the period was divided into two stages. Both of them were characterized of the bottom water SSC increasing first and then descending. The SSC reached the maximum at 2:00 on September 24 (10.56 g/L) and at 15:00 on September 24 (17.25 g/L), respectively. These two stages share a similar pattern that the SSCs in the upper layers (the distances from the ground greater than 30 cm) increase earlier than the bottom water (Figs 6d and f). When the SSC at the upper layers reaches a certain value (about 3 g/L), the SSC at the bottom began to increase. In the decreasing phase, the concentration of suspended sediment in the bottom decreases firstly.

Because of the hydrodynamic effect was weak at low tide level, the SSC in water was very small, almost 0. The vertical distribution of SSC was only studied at high tide. The vertical distribution of SSC (< 96 cm from the seabed) shows the SSC increased from the surface to the bottom (Fig. 7), and the fitting curve appeared exponential distribution. The fitting curve equation is

$$y = a + be^{-cx}. \tag{15}$$

As the limitation of the observation instrument, we can only get the SSC data within 96 cm above the seabed. Because of the SSC change in upper layer was very small, almost 0, we could calculated the SSC that was not observed. We put together all the

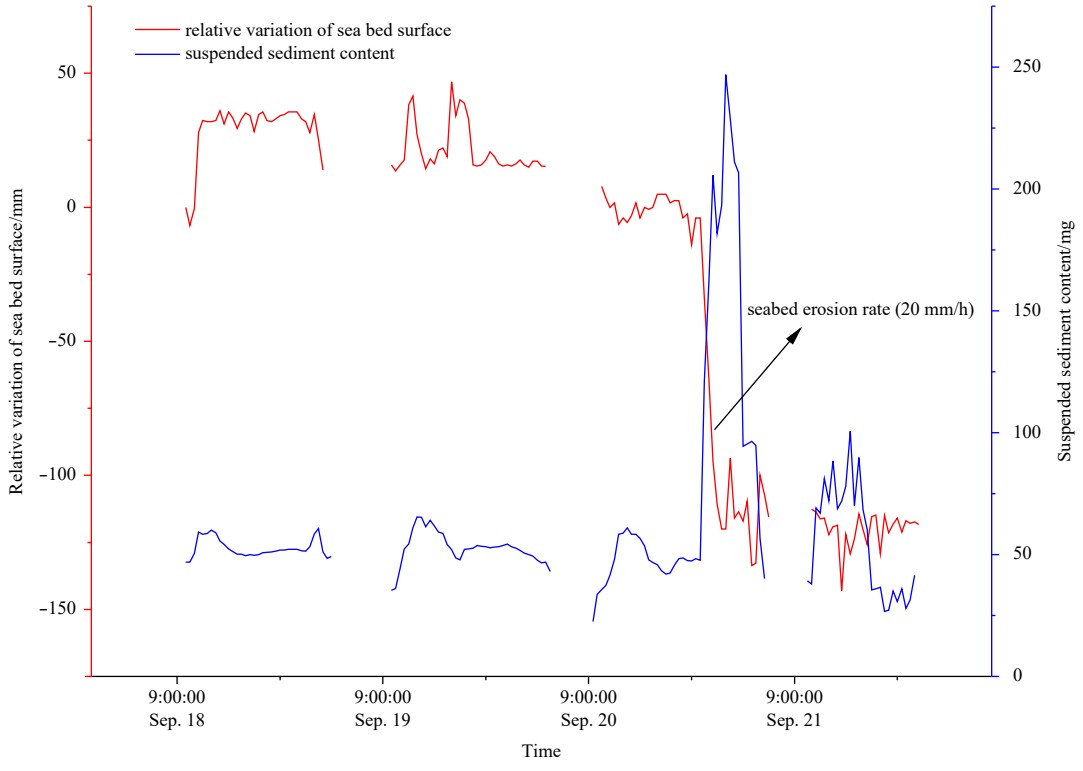

Fig. 5. The relative variations of sea bed surface from September 18 to 21.

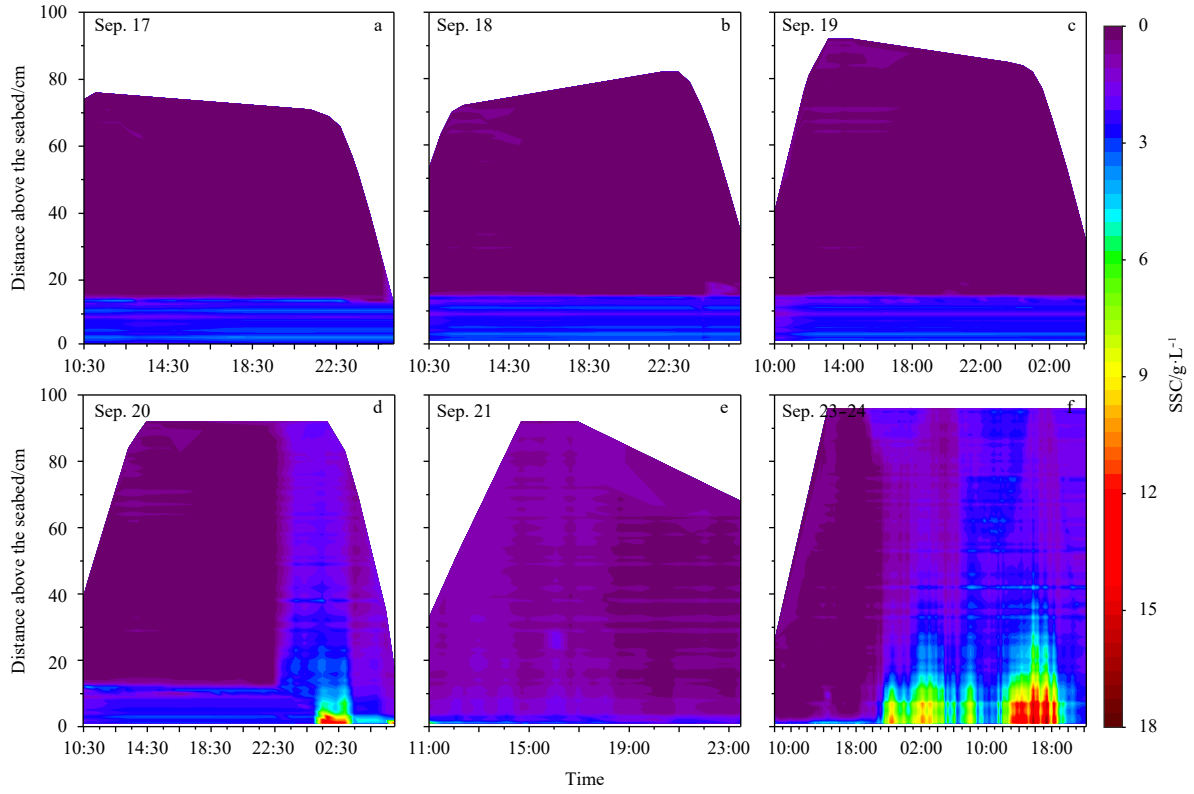

Fig. 6. SSC from September 17 to 18 (a), September 18 to 19 (b), September 19 to 20 (c), September 20 to 21 (d), on September 21 (e), and September 23 to 24 (f).

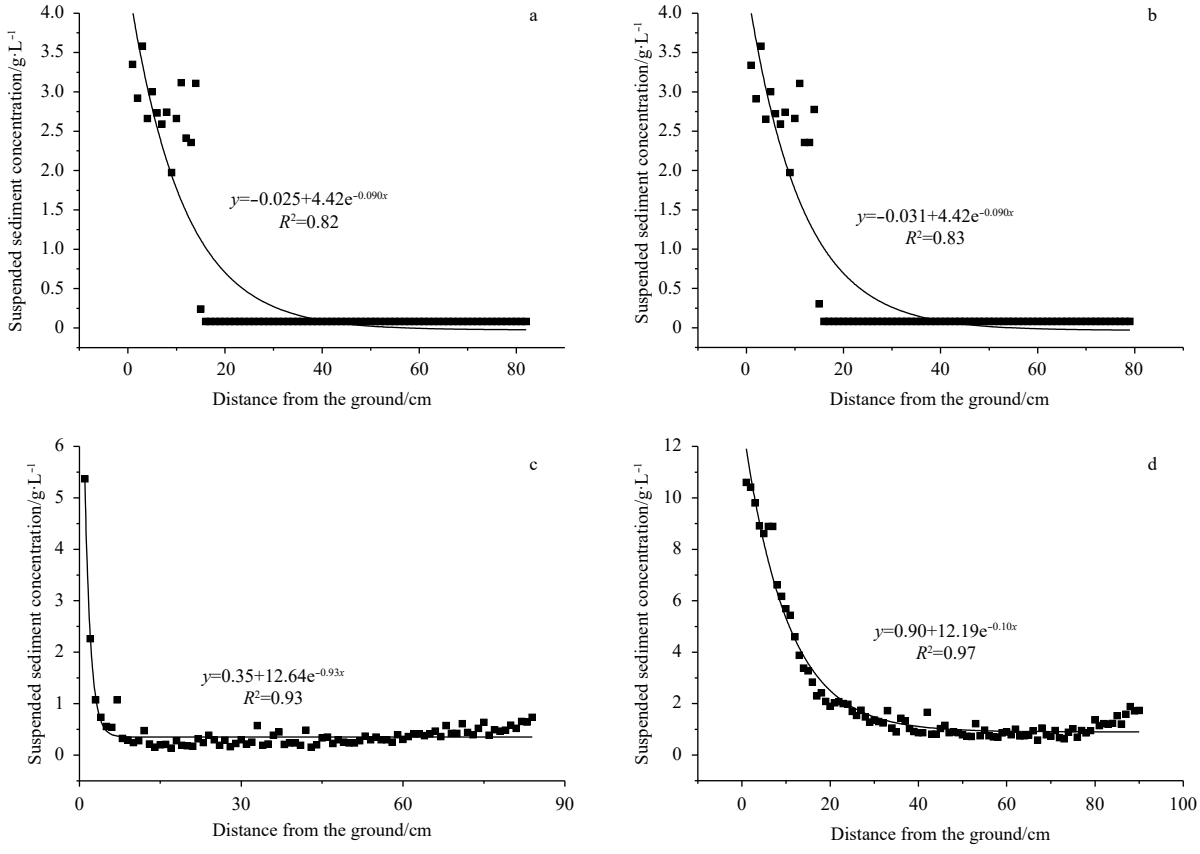

Fig. 7. The vertical distribution of turbidity at 23:00 on September 19 (a), 13:00 on September 20 (b), 22:00 on September 23 (c), and 2:00 on September 24 (d).

SSC at different depths to represent the suspended sediment content in the whole water column that the area of base was 1 cm×1 cm. The suspended sediment content change with hydrodynamic. Figure 4 shows the hydrodynamic was stronger during the period from September 21 to 24. The suspended sediment content increased with wave height during the four periods, namely 1:00–4:00 on September 21, 12:30–22:30 on September 23, 1:30–8:30 and 13:30–20:30 on September 24. The maximums of significant wave height were more than 0.3 m during the four periods. During the two-period on September 21 and 23, the suspended sediment content was respectively 300 mg and 462 mg. From the above analysis, it suggests that the variation of suspended sediment content is mainly affected by wave, which was consistent with the observations results in the Huanghe River subaqueous delta (Yang et al., 2011). The suspended sediment content peaks appeared before and after the current velocity peaks. These showed that the fluctuation in a trend of suspended sediment concentration variation is mainly affected by tidal current.

Based on the analysis of the process of suspended sediment content change and suspended sediment content peaks, it was founded that the suspended sediment increased with the wave height increased. It showed that the wave plays a major role in the change of suspended sediment content. While the suspended sediment content peaks appeared with current velocity peaks appeared. It showed that the current plays a role in the change of suspended sediment content in the Huanghe River Estuary intertidal flat during the observation period.

5 Discussion

Studies have shown that suspended sediments in the Huanghe River intertidal flat are composed of transport sediments, wave-induced resuspended sediments and current-induced resuspended sediments. It is necessary to separate the three for analyzing the specific contribution of different dynamic effects to suspended sediments, and the study of the relationship between suspended sediment flux and hydrodynamics is helpful to analyze the composition of advective sediment in suspended sediment.

The suspended sediment content correlates with shear stress calculated by Eq. (3) (Li et al., 2020a) under smooth-wavelet, while under the calm-rippled is opposite (Fig. 8). It indicates that the sediment resuspension did not occur under calm-rippled, which occurred mostly under smooth-wavelet.

When the shear stress was less than the critical shear stress (0.30 Pa) (Li et al., 2016), the average suspended sediment content in water was 52.22 mg. The equation of the correlation between suspended sediment fluxes and hydrodynamic could be expressed:

$$T = 52.22VA, \tag{16}$$

where T is the suspended sediment flux (mg/s); V is the current velocity (cm/s); and A is the unit area, assumed to be 1 cm^2.

When the shear stress was more than the critical shear stress (0.30 Pa), the most time of the observation period was smooth-wavelet. Based on the formula of correlation between SSC and wave, the equation of the correlation between suspended sediment fluxes and hydrodynamic may be expressed:

$$T = (29.23 + 124.36\tau)\, VA = 29.23VA + 124.36\tau VA, \tag{17}$$

where τ is total shear stress (Pa).

The equation is corrected based on the correlation between observed suspended sediment flux and calculated flux (Fig. 9). When the shear stress is less than the critical shear stress (0.30 Pa), the corrected equation is

$$T = 0.99 \times 52.22V - 2.58 = 51.70V - 2.58. \tag{18}$$

The equation is corrected based on the correlation between observed suspended sediment flux and calculated flux (Fig. 9). When the shear stress is more than the critical shear stress (0.30 Pa), the corrected equation is

$$\begin{aligned} T &= 0.98 \times (29.23V + 124.36\tau V) - 4.24 \\ &= 28.65V + 121.87\tau V - 4.24. \end{aligned} \tag{19}$$

Based on this, when the shear stress is less than the critical shear stress (0.30 Pa), the suspended sediment flux is mainly controlled by the current velocity (tidal current and Stokes drift). While the shear stress is more than the critical shear stress, the shear stress induced by waves and tidal currents also affects the variation of suspended sediment flux through affecting SSC.

Because of the SSC varies lightly if sediment is not resuspended, Eqs (4) and (5) could be used to differentiate suspended sediment content source from sediment transport or local resuspension. The calculated results (Table 1) show that the directions of average velocity are the same as the advection transport in each tidal cycle. Net landward sediment transported from the

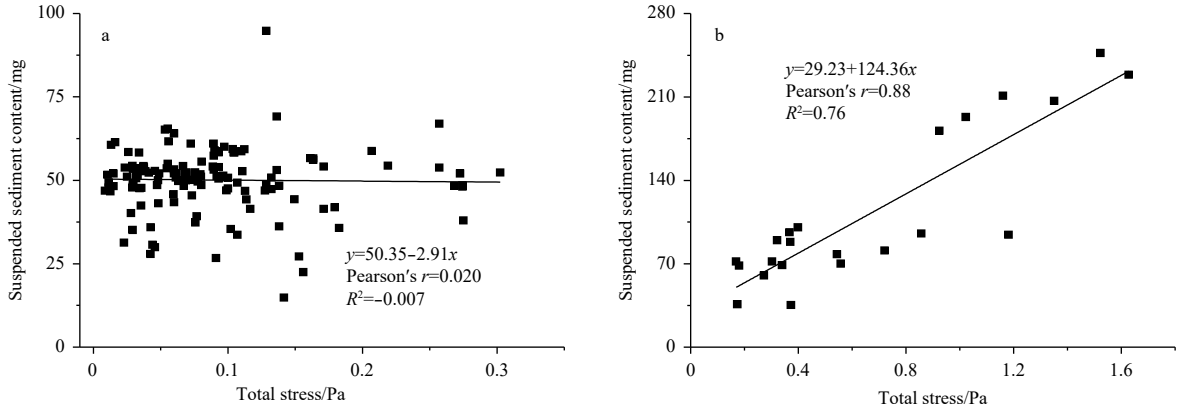

Fig. 8. Suspended sediment content changes with total stress under calm-rippled (a) and smooth-wavelet (b).

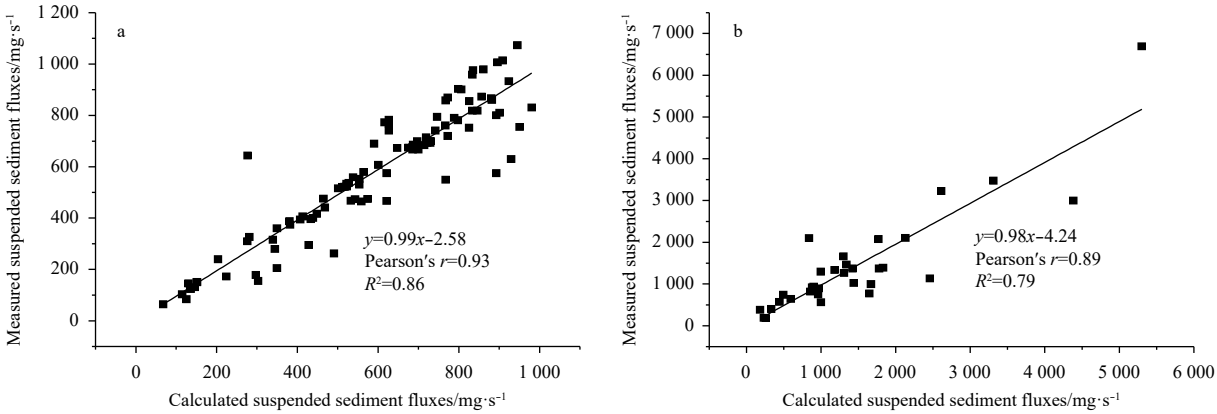

Fig. 9. The correlation between calculated value and measured value. a. The shear stress is less than the critical shear stress (0.21 Pa); and b. the shear stress is more than the critical shear stress (0.21 Pa).

intertidal flat, when the flood tide dominated. Apart from the two tidal cycles from 20:00 September 20 to 6:00 September 21 and from 8:00 to 23:30 September 23, advection transport volumes or Stokes Drift volumes are more than resuspended sediment content. The calculated results coincide with the observation results of relative variation of the sea bed surface (Fig. 5). They illustrate sediment transport is the main source of suspended sediment in the Huanghe River Estuary tidal flat. The effect is 1–3 times as much as resuspension. But if the seabed suffers large-scale erosion (the erosion depth greater than 100 mm) when hydrodynamics are enhanced in a tidy cycle, the resuspended sediment may become the main source of suspended sediment. This phenomenon is resulted by the resuspended sediments caused by waves in the tidal flat remain in a suspended state and are transported by the dominant current under the action of the tidal current, but after a large erosion of the seabed, offshore transports of suspended sediment are enhanced (Christie et al., 1999), due to the lag effect of sediment change at the intertidal flat (Li et al., 2020b). This also explains that the suspended sediment offshore transport at the Dollard Estuary in the Netherlands is significantly strengthened during storm surges (De Haas and Eisma, 1993). However, in the Willapa Bay, Washington, USA, stroms enhance suspended sediment onshore transport, due to the ebb tidal strength decrease significantly with the increase of wind speed, and the flood tidal strength increase slightly with the increase of wind speed (Nowacki and Ogston, 2013).

During the period of observation, under calm-rippled condition, the fraction of resuspended sediment mobilized by currents was much greater than the fraction mobilized by wave (Fig. 10a). The most of wave-induced suspended sediment contents were less than 10 mg, and the current-induced suspended sediment was up to 25.50 mg. Under the smooth-wavelet condition, the fraction of resuspended sediment mobilized by waves was much greater than the current (Fig. 10b). The most of current-induced suspended sediment were less than 10 mg, and the wave-induced suspended sediment was up to 99.24 mg. Janssen-Stelder (2000) use the Van Rijn (1990) model to analyze the wave and tidal components in the total shear stress, and also find that in calm weather conditions, the tidal component is slightly higher than the wave component; during a storm, with the total stress increases, the contribution of waves to the total stress increases (up to 81%). It shows that the control factors of sediment resuspension under different sea conditions in the same area are also different. Therefore, in the subsequent research, it is necessary to analysis the control factors of sediment resuspension under other sea conditions in the Huanghe River Estuary, especially under the action of storm.

6 Conclusions

Based on 7-d hydrodynamic observations data (water depth, wave height, and current velocity) and SSC measurements on the tidal flat off the Huanghe River Mouth, the correlation between

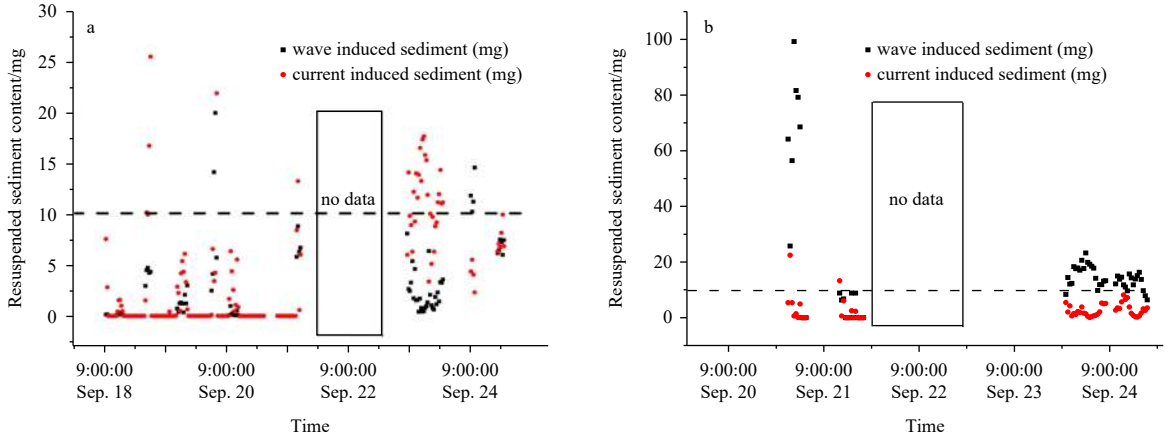

Fig. 10. The contribution of waves and currents to resuspension in calm-rippled (a) and smooth-wavelet (b).

suspended sediment and hydrodynamic conditions are further revealed. The main conclusions are as follows:

(1) The *in-situ* records showed that sea conditions were mainly calm-rippled to smooth-wavelet. When the hydrodynamics enhanced, the SSC in the upper layers increased from 0.1 g/L to 3.0 g/L, and the SSC at the bottom increased from 1–3 g/L to 17.3 g/L.

(2) The suspended sediment flux is mainly controlled by the tidal current and Stokes drift, while the wave-induced shear stress could also affect the variation of suspended sediment flux. The resuspended sediments caused by waves in the tidal flat remain in a suspended state and are transported by the dominant current under the action of the tidal current, but after a large erosion of the seabed, offshore transports of suspended sediment are enhanced, due to the lag effect of settlement

(3) Advection transport sediment and Stokes drift transport sediment from the river are the main source of suspended sediment, while the seabed suffer large-scale erosion (a single smooth-wavelet event could cause 11.8 cm seabed erosion within 6 h) when hydrodynamics are enhanced in a tidy cycle, and resuspended sediment becomes the main source of suspended sediment.

(4) When sea under calm-rippled conditions, the current-induced resuspended sediment concentration (RSC) was greater than the wave-induced RSC. In contrast, in smooth-wavelet sea conditions, the wave-induced SSC was greater than the current-induced SSC.

Acknowledgements

Special thanks go to the Ocean University of China for the joint training MSc programs and NC State University giving me a visiting scholar chance. Thanks go to Fudong Ji for their assistance with fieldwork.

References

Andersen T J, Pejrup M. 2001. Suspended sediment transport on a temperate, microtidal mudflat, the Danish Wadden Sea. Marine Geology, 173(1–4): 69–85, doi: 10.1016/S0025-3227(00)00164-X

Chen Jianyong, Dai Zhijun, Chen Jiyu, et al. 2009. Analysis on the net sediment transportation along arc-shaped coast in the northern bank, Hangzhou bay—a case study of Longquan-Nanzhu harbor segment. Journal of Sediment Research (in Chinese), (2): 53–59

Chen Bin, Gao Fei, Liu Jian. 2017. Sediment transport mechanism in the Zhejiang inner continental shelf in summer. Haiyang Xuebao (in Chinese), 39(3): 96–105

Chen Shenliang, Gu Guochuan, Zhang Guoan. 2003a. Settling velocity of suspended sediment in the Nanhui nearshore waters of Changjiang estuary. Journal of Sediment Research (in Chinese), (6): 45–51

Chen Shenliang, Zhang Guoan, Yang Shilun. 2003b. Temporal and spatial changes of suspended sediment concentration and resuspension in the Yangtze River estuary. Journal of Geographical Sciences, 13(4): 498–506, doi: 10.1007/BF02837889

Chen Shenliang, Zhang Guoan, Yang Shilun, et al. 2004. Temporal and spatial changes of suspended sediment concentration and resuspension in the Yangtze River Estuary and its adjacent waters. Acta Geographica Sinica (in Chinese), 59(2): 260–266

Cheng Guodong, Xue Chunting. 1997. Sedimentary Geology in the Yellow River Delta (in Chinese). Beijing: Geological Publishing House

Christie M C, Dyer K R, Turner P. 1999. Sediment flux and bed level measurements from a macro tidal mudflat. Estuarine, Coastal and Shelf Science, 49(5): 667–688, doi: 10.1006/ecss.1999.0525

De Haas H, Eisma D. 1993. Suspended-sediment transport in the Dollard estuary. Netherlands Journal of Sea Research, 31(1): 37–42, doi: 10.1016/0077-7579(93)90014-J

Grant W D, Madsen O S. 1979. Combined wave and current interaction with a rough bottom. Journal of Geophysical Research: Oceans, 84(C4): 1797–1808, doi: 10.1029/JC084iC04p01797

Green M O. 2011. Very small waves and associated sediment resuspension on an estuarine intertidal flat. Estuarine, Coastal and Shelf Science, 93(4): 449–459, doi: 10.1016/j.ecss.2011.05.021

Guo Lei, Wen Mingzheng, Shan Hongxian, et al. 2016. Study on resuspension process of seabed sediment induced by wave. Marine Geology & Quaternary Geology (in Chinese), 36(5): 181–188

He Songlin, Sun Jiemin. 1996. Characteristics of suspended sediment transport in the turbidity maximum of the Changjiang River estuary. Oceanologia et Limnologia Sinica (in Chinese), 27(1): 60–66

Hu Chunhong, Ji Zuwen, Wang Tao. 1996. Characteristics of ocean dynamics and sediment diffusion in the Yellow River estuary. Journal of Sediment Research (in Chinese), (4): 1–10

Janssen-Stelder B. 2000. The effect of different hydrodynamic conditions on the morphodynamics of a tidal mudflat in the Dutch Wadden Sea. Continental Shelf Research, 20(12–13): 1461–1478, doi: 10.1016/S0278-4343(00)00032-7

Jay D A, Uncles R J, Largeir J, et al. 1997. A review of recent developments in estuarine scalar flux estimation. Estuaries, 20(2): 262–280, doi: 10.2307/1352342

Kineke G C, Sternberg R W. 1992. Measurements of high concentration suspended sediments using the optical backscatterance sensor. Marine Geology, 108(3–4): 253–258, doi: 10.1016/0025-3227(92)90199-R

Kong Yazhen, Ding Pingxing, He Songlin, et al. 2006. Analysis of spatial and temporal variation characteristics of suspended sediment concentration in the Changjiang River Eatuary and adjacent sea area. Advances in Marine Science (in Chinese), 24(4): 446–454

Lavelle J W, Mofjeld H O, Baker E T. 1984. An in situ erosion rate for a fine-grained marine sediment. Journal of Geophysical Research: Oceans, 89(C4): 6543–6552, doi: 10.1029/JC089iC04p06543

Li Bowen, Jia Yonggang, Liu J P, et al. 2020a. Effect of wave, current, and lutocline on sediment resuspension in Yellow River delta-front. Water, 12(3): 845, doi: 10.3390/w12030845

Li Bowen, Jia Yonggang, Zhang Ying, et al. 2020b. Study on processes of seabed in the Yellow River Delta. Journal of Sediment Research (in Chinese), 45(2): 16–22

Li Bowen, Shan Hongxian, Zhang Shaotong, et al. 2016. Contribution of waves and currents to sediment suspension revealed by in-situ observation. Marine Geology & Quaternary Geology (in Chinese), 36(3): 183–190

Li Guangxue, Wei Helong, Han Yeshen, et al. 1998a. Sedimentation in the Yellow River delta, part I: flow and suspended sediment structure in the upper distributary and the estuary. Marine Geology, 149(1–4): 93–111, doi: 10.1016/S0025-3227(98)00031-0

Li Guangxue, Wei Helong, Yue Shuhong, et al. 1998b. Sedimentation in the Yellow River delta, part II: suspended sediment dispersal and deposition on the subaqueous delta. Marine Geology, 149(1–4): 113–131, doi: 10.1016/S0025-3227(98)00032-2

Liu Xiaolei, Jia Yonggang, Zheng Jiewen, et al. 2013. Field and laboratory resistivity monitoring of sediment consolidation in China's Yellow River estuary. Engineering Geology, 164: 77–85, doi: 10.1016/j.enggeo.2013.06.009

Lund-Hansen L C, Valeur J, Pejrup M, et al. 1997. Sediment fluxes, resuspension and accumulation rates at two wind-exposed coastal sites and in a sheltered bay. Estuarine, Coastal and Shelf Science, 44(5): 521–531, doi: 10.1006/ecss.1996.0163

Nowacki D J, Ogston A S. 2013. Water and sediment transport of channel-flat systems in a mesotidal mudflat: Willapa Bay, Washington. Continental Shelf Research, 60(15): S111–S124

Pejrup M. 1988. Suspended sediment transport across a tidal flat. Marine Geology, 82(3–4): 187–198, doi: 10.1016/0025-3227(88)90140-5

Prior D B, Suhayda J, Lu N Z, et al. 1989. Storm wave reactivation of a

submarine landslide. Nature, 341(6237): 47–50, doi: 10.1038/341047a0

Ramaswamy V, Rao P S, Rao K H, T, et al. 2004. Tidal influence on suspended sediment distribution and dispersal in the northern Andaman Sea and Gulf of Martaban. Marine Geology, 208(1): 33–42, doi: 10.1016/j.margeo.2004.04.019

Ren Huiru, Li Guosheng, Guo Tengjiao, et al. 2017. Multi-scale variability of surface wind direction and speed on the Bohai Sea in 1950–2011. Scientia Geographica Sinica (in Chinese), 37(9): 1430–1438

Ren Meie, Shi Yunliang. 1986. Sediment discharge of the Yellow River (China) and its effect on the sedimentation of the Bohai and the Yellow Sea. Continental Shelf Research, 6(6): 785–810, doi: 10.1016/0278-4343(86)90037-3

Roman M R, Tenore K R. 1978. Tidal resuspension in Buzzards Bay, Massachusetts: I. Seasonal changes in the resuspension of organic carbon and chlorophyll a. Estuarine and Coastal Marine Science, 6(1): 37–46

Rose C P, Thorne P D. 2001. Measurements of suspended sediment transport parameters in a tidal estuary. Continental Shelf Research, 21(15): 1551–1575, doi: 10.1016/S0278-4343(00)00087-X

Shi N C, Larsen L H, Downing J P. 1985. Predicting suspended sediment concentration on continental shelves. Marine Geology, 62(3–4): 255–275, doi: 10.1016/0025-3227(85)90119-7

Shi Zhong, Ling Honglie. 1999. Vertical profiles of fine suspension concentration in the Changjiang esturary. Journal of Sdeiment Research (in Chinese), (2): 59–64

Sternberg R W, Berhane I, Ogston A S. 1999. Measurement of size and settling velocity of suspended aggregates on the northern California continental shelf. Marine Geology, 154(1–4): 43–53, doi: 10.1016/S0025-3227(98)00102-9

Thompson C E L, Couceiro F, Fones G R, et al. 2011. In situ flume measurements of resuspension in the North Sea. Estuarine, Coastal and Shelf Science, 94(1): 77–88, doi: 10.1016/j.ecss.2011.05.026

Van Rijn L C. 1990. Principles of Fluid Flow and Surface Waves in Rivers, Estuaries, Seas, and Oceans. Amsterdam, The Netherlands: Aqua Publications

Wan Xinning, Li Jiufa, Shen Huanting. 2006. Distribution and diffusion of suspended sediment in the offshore area of Changjiang Estuary, China. Geographical Research (in Chinese), 25(2): 294–302

Wang Ying, Aubrey D G. 1987. The characteristics of the China coastline. Continental Shelf Research, 7(4): 329–349, doi: 10.1016/0278-4343(87)90104-X

Wang Hailong, Han Shuzong, Guo Peifang, et al. 2011. Transportation of sediment from Yellow River in Bohai Sea due to tidal currents. Journal of Sediment Research (in Chinese), (1): 51–59

Wang Yangui, Hu Chunhong, Zhu Bisheng. 2007. Study on formula of incipient velocity of sediment in model test. Journal of Hydraulic Engineering (in Chinese), 38(5): 518–523

Wright L D, Boon J D, Xu J P, et al. 1992. The bottom boundary layer of the bay stem plains environment of lower Chesapeake Bay. Estuarine, Coastal and Shelf Science, 35(1): 17–36, doi: 10.1016/S0272-7714(05)80054-X

Wright L D, Nittrouer C A. 1995. Dispersal of river sediments in coastal seas: six contrasting cases. Estuaries, 18(3): 494–508, doi: 10.2307/1352367

Wright L D, Sherwood C R, Sternberg R W. 1997. Field measurements of fairweather bottom boundary layer processes and sediment suspension on the Louisiana inner continental shelf. Marine Geology, 140(3–4): 329–345, doi: 10.1016/S0025-3227(97)00032-7

Wright L D, Wiseman W J, Bornhold B D, et al. 1988. Marine dispersal and deposition of Yellow River silts by gravity-driven underflows. Nature, 332(6165): 629–632, doi: 10.1038/332629a0

Wright L D, Wiseman W J Jr, Yang Z S, et al. 1990. Processes of marine dispersal and deposition of suspended silts off the modern mouth of the Huanghe (Yellow River). Continental Shelf Research, 10(1): 1–40, doi: 10.1016/0278-4343(90)90033-I

Wu Dean, Zhang Renshun, Yan Yixin, et al. 2006. Mechanism of suspended sediment transport in Dongdagang tidal channel of radial sand ridges. Journal of Hohai University (Natural Sciences) (in Chinese), 34(2): 216–222

Yang Zuosheng, Ji Youjun, Bi Naishuang, et al. 2011. Sediment transport off the Huanghe (Yellow River) delta and in the adjacent Bohai Sea in winter and seasonal comparison. Estuarine, Coastal and Shelf Science, 93(3): 173–181, doi: 10.1016/j.ecss.2010.06.005

You Zaijin. 2005. Fine sediment resuspension dynamics in a large semi-enclosed bay. Ocean Engineering, 32(16): 1982–1993, doi: 10.1016/j.oceaneng.2005.01.006

Zhang Yansong, Zhang Feijun, Guo Xuewu, et al. 2004. Vertical flux of the settling particulate matter in the water column of the Yellow Sea in summer. Oceanologia et Limnologia Sinica (in Chinese), 35(3): 230–238

Zhang Yansong, Zhang Feijun, Guo Xuewu, et al. 2005. Autumn vertical flux of settling particulate matter at three typical stations in the Yellow Sea. Geochimica (in Chinese), 34(2): 123–128

Zhao Dongbo. 2004. The study of the erosion of Diaokou course coast in Yellow River delta (in Chinese) [dissertation]. Qingdao: Ocean University of China, 1–75

Zhou Liangyong, Chen Bin, Liu Jian, et al. 2009. Observation of currents and suspended sediment concentration off northern Jiangsu coast, China. Marine Geology & Quaternary Geology (in Chinese), 29(6): 17–24

Zong Haibo. 2009. Wind wave induced sediment resuspension in the Yellow River mouth (in Chinese) [dissertation]. Qingdao: Ocean Univeristy of China, 1–55

Zuo Shuhua, Li Jiufa, Wan Xinning, et al. 2006. Characteristics of temporal and spatial variation of suspended sediment concentration in the Changjiang Estuary. Journal of Sediment Research (in Chinese), (3): 68–75